

Supporting Information

Table S1: Fly line used in this study

Line No.	Genotype	Origin
BL-35514	w[*];P(4-10,27,30)9.1	(Katsani et al., 2008)
dElys ^{KK} (v103547)	P{KK100932}VIE-260B	VDRC
dElys ^{TRiP}	Y ¹ V ¹ ;p{pVALIUM10_dElys-1}/Cyo;attp40	This Study (TRiP based)
EYFP-dELYS	W[*],p{pTVW-dElys}	This Study
BL-53269	y1 sc* v1; P{TRiP.HMC02426}attP2	(27)
BL-25374	y1 w*; P{Act5C-GAL4-w}E1/CyO	BDSC
BL-5534	w*; P{GAL4-ey.H}3-8	BDSC
BL-25754	P{UAS-Dcr-2.D}1, w1118; P{GawB}nubbin-AC-62	BDSC
BL-1561	w*; P{GAL4-arm.S}4a P{GAL4-arm.S}4b/TM3, Sb1 Ser1	BDSC
BL-7062	w[*]; P{w[+mC]=matalpha4-GAL-VP16}V2H	BDSC
BL-6657	w[*]; P{w[+mC]=UAS-DIAP1.H}3	BDSC
	dElys ^{KK} ; UAS-DIAP1	This Study
v105491 (Dorsal RNAi)	P{KK107820}VIE-260B	VDRC
	dElys ^{KK} ; Dorsal ^{RNAi}	This Study
v21937 (Nup160 RNAi)	w[1118]; P{GD11413}v21937	VDRC
v110194 (Nup133 RNAi)	P{KK102392}VIE-260B	VDRC
V22407 (Nup107 RNAi)	w[1118]; P{GD12024}v22407	VDRC
BL-32837 (Nup153 RNAi)	y[1] sc[*] v[1]; P{y[+t7.7] [+t1.8]=TRiP.HMS00527}attP2	BDSC
BL-47326 (fkh-GAL4)	w[1118]; P{y[+t7.7] w[+mC]=GMR16E04-GAL4}attP2	BDSC
BL-6979 (C147-GAL4)	w[1118]; P{w[+mW.hs]=GawB}C147	BDSC
	w[1118];C147-GAL4;fkh-GAL4	This study

BL-4775	w[1118]; P{w[+mC]=UAS-GFP.nls}14	BDSC
	Nucleoporin RNAi; UAS-GFP-NLS	This study
BL-7096	dl[4] pr[1] cn[1] wx[wxt] bw[1]/CyO	BDSC
	UAS- <i>dElys</i> ; <i>dElys</i> ^{KK}	This study

Table S2: Primer used in this study

Primer Name	Sequence
<i>dElys</i> _1_F	5-ATTCCCGGGTATGGAGTGGCACGAAGTGGAGTTGG-3'
<i>dElys</i> _2111_R	5' -ATCGCGGCCGCCTAATGCTCCGACTTGGAGGTG-3'
<i>dElys</i> _1769_F	5' -ATCGAATTCCAGTCTAGTGGTCTTGGGG-3'
Nup43_F	5' -ATCGAATTCCAATCGAACCAATATGTCACC-3'
Nup43_R	5' -ATCCTCGAGTTAATTTTCCACGGAGACGATGC-3'
AT-hook_F	5'-CAGGAATTCTTGCGACCGCGTCG-3'
AT-hook_R	5'-CAGCTCGAGCTAGCCGGGTCTGGAG-3'
AT-hook_mAT-1_F	5'-CGAACTCTGGCACCTGCTGCCGTCTCC-3'
AT-hook_mAT-1_R	5'- GGAGACGGCAGCAGGTGCCAGAGTTCCG-3'
AT-hook_mAT-2_F	5'-ACTCCCAAGGCTGCTGGGTTGCAGCAC-3'
AT-hook_mAT-2_R	5'-GTGCTGCAACCCAGCAGCCTTGGGAGT-3'
AT-hook_mAT-3_F	5'-CCGGCCACCGCCTCGGCAACGCGCCTC-3'
AT-hook_mAT-3_R	5'-GAGGCGCGTTGCCGAGGCGGTGGCCGG-3'
<i>dElys</i> _gateway_F	5'-CACCATGGAGTGGCACGAAGTGGAG-3'
<i>dElys</i> _gateway_R	5'-CTAATGCTCCGACTTGGAGG-3'
<i>dElys</i> _NLS_F	5'-CACCGACCAGAGGCAGC-3'
<i>dElys</i> _NLS_R	5'-AGTTCGCAGAGGAATGG-3'
<i>dElys</i> _NES_F	5'-CACCGCGGTGCCGGACG-3'
<i>dElys</i> _NES_R	5'-TTCCAACCTCCGGCAC-3'

dElys_RT_F	5'-GATGAGGAGGAGCAAGATGTG-3'
dElys_RT_R	5'-TTGGATGCGGGCGATAAA-3'
RpL49_F	5'-CGTTTACTGCGGCGAGAT-3'
RpL49_R	5'-GTGTATTCCGACCACGTTACA-3'
Nup153_RT_F	5'-GCACCAAAGGTCAACAACCTTC-3'
Nup153_RT_R	5'-GGGAGTCGCAACAGCTATATT-3'
dElys_TRiP_F	5'-CACCTGGAGCCCTACCAAAAGAC-3'
dElys_TRiP_R	5'-CGCCTGGAGGAAATTTGG-3'
CG15643_RT_F	5'- ACTGCGTTCACCTTCTACTG-3'
CG15643_RT_R	5'-CCTAAAGCGATCCCTGACTTAG-3'
CG7051_RT_F	5'-CCTTGGTCTCCCAAACCTCTTC-3'
CG7051_RT_R	5'-CCGGTTCACCGTCACAATAA-3'
Reaper_RT_F	5'-CGGAAGAAAGTCCGGCAAATA-3'
Reaper_RT_R	5'-GTTGTGGCTCTGTGTCCTT-3'
Hid_RT_F	5'-CGATTGAAATTTGGCCAGAAGAG -3'
Hid_RT_R	5'-GCCCGGGAAATTCTAGCATATAG-3'
DIAP-1_RT_F	5'-GCCGGCGACAAAGTTAAATG-3'
DIAP-1_RT_R	5'-GCCGCAGATATCGTAGCTTATT-3'
Snail_RT_F	5'-CTCATCGGGATACTCCTACACT-3'
Snail_RT_R	5'-GTGGGTCTTCTTCTCCTGATTAC-3'
Twist_RT_F	5'-CCAGCAACAGATCTATGTGGATTA-3'
Twist_RT_R	5'-TGCTGCTGGTTGTTGTAGAG-3'
Rho_RT_F	5'-GAACTAATCGCCTCTCGCTATG-3'
Rho_RT_R	5'-ATCCTACAATTCGGAGCACATT-3'

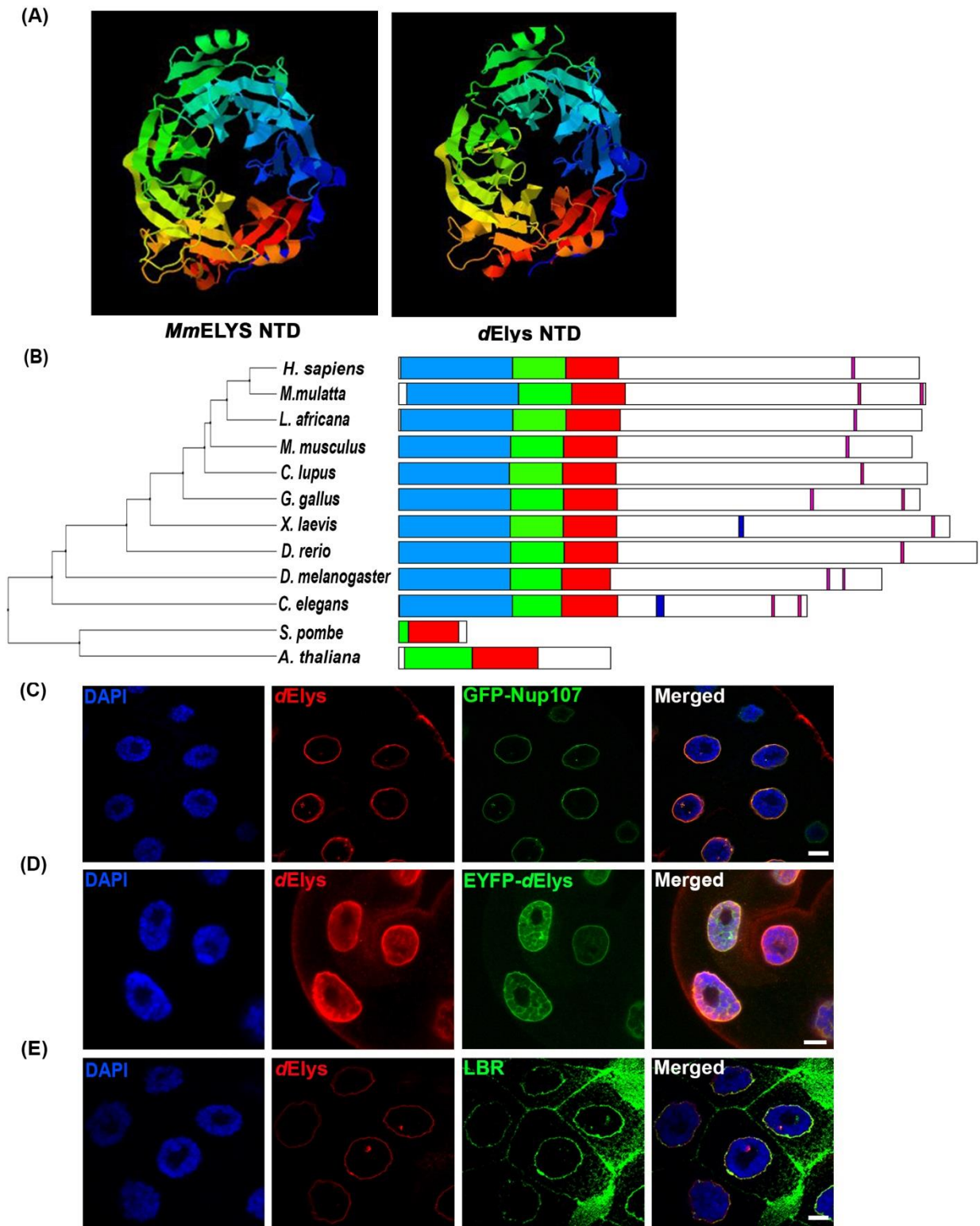


Figure S1: *dElys* is structurally conserved and show nuclear rim co-localization with Nup107 and LBR

(A) Modeling of N-terminal domain of *dElys* modeled using Phyre2 software and compared with mouse ELYS N-terminal domain.

(B) Phylogenetic analysis of ELYS orthologues from yeast, invertebrates, vertebrates, and plants. Domain structure of ELYS represented as β -sheet containing N-terminal domain (blue), α -helical central domain (green), conserved ELYS domain (red), coiled-coil domain (dark blue) and AT-hook like DNA binding motifs (purple).

(C) Anti-*dElys* serum (red) used for staining on the third instar larval salivary gland from GFP-Nup107 (green) expressing larva. DNA is stained with DAPI. (Scale bar: 10 μ m)

(D) EYFP tagged *dElys* (green) expressed in third instar larval *Drosophila* salivary gland nuclei located on the nuclear periphery. DNA is stained with DAPI. (Scale bar: 5 μ m)

(E) Localization of *dElys* (red) and Lamin B receptor (LBR) (green) at the nuclear rim in third instar larval *Drosophila* salivary glands. DNA is stained with DAPI. (Scale bar: 5 μ m)

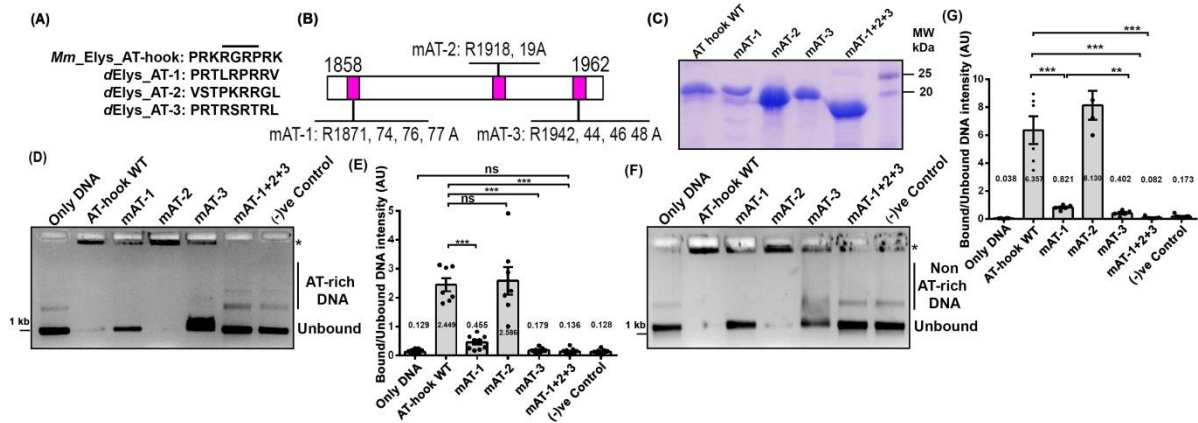


Figure S2: dElys AT-hook like motifs are functional

(A) Three predicted AT-hook like DNA binding motifs of CG14215 are compared with the canonical mouse AT-hook motif. Core -RGRP- signature residues of AT-hook are marked.

(B) Graphical representation of the position of each AT-hook like motif of dElys in fragment cloned for protein purification. Conserved arginine residues were mutated to alanine, and the position of each arginine residue is indicated.

(C) The SDS-PAGE analysis of purified wild-type and mutant AT-hook like proteins used for the DNA binding experiment. Molecular weight markers are indicated next to the gel.

(D) DNA binding ability of predicted AT-hook like motifs is tested in the EMSA experiment. AT-rich DNA binding by purified AT-hook like fragment (AA. 1858-1962) and mutated AT-hook proteins where arginines mutated to alanines are shown. The type of protein used is indicated above each lane. An asterisk indicates bound DNA with decreased mobility.

(F) Non-AT rich DNA binding ability of predicted AT-hook like motifs is tested in the EMSA experiment. A variant of protein used in the reaction is indicated above each lane. An asterisk indicates bound DNA with decreased mobility.

(E, G) Quantification of AT-rich DNA (E) and Non-ATrich DNA (G) binding ability of each AT-hook like fragment used. Quantification is derived from at least three independent experiments. Quantification values are mentioned with each bar. *** represents $p < 0.0001$, ns is non-significant. Error bars represent standard error of the mean (SEM). Statistical analysis is derived from one-way ANOVA followed by post-hoc Tukey's multiple comparison tests.

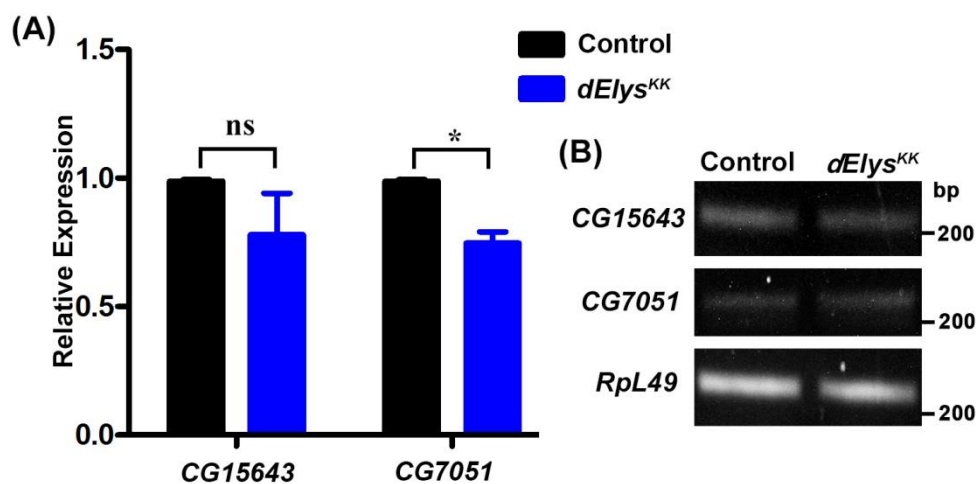


Figure S3: Expression analysis of predicted off-targets of the *dElys^{KK}* RNAi line

(A) Graphical representation of quantitative PCR showing the expression level of predicted off-targets (*CG15643* and *CG7051*) of the *dElys^{KK}* RNAi line from VDRRC. Data are represented from at least five independent experiments. Statistical significance derived from the student's t-test. The error bars represent the standard deviation. * represents $p < 0.05$, ns is non-significant.

(B) Semi-quantitative PCR analysis of *dElys^{KK}* RNAi line off-targets. *RpL49* was used as an internal control gene. Data are derived from at least three independent experiments.

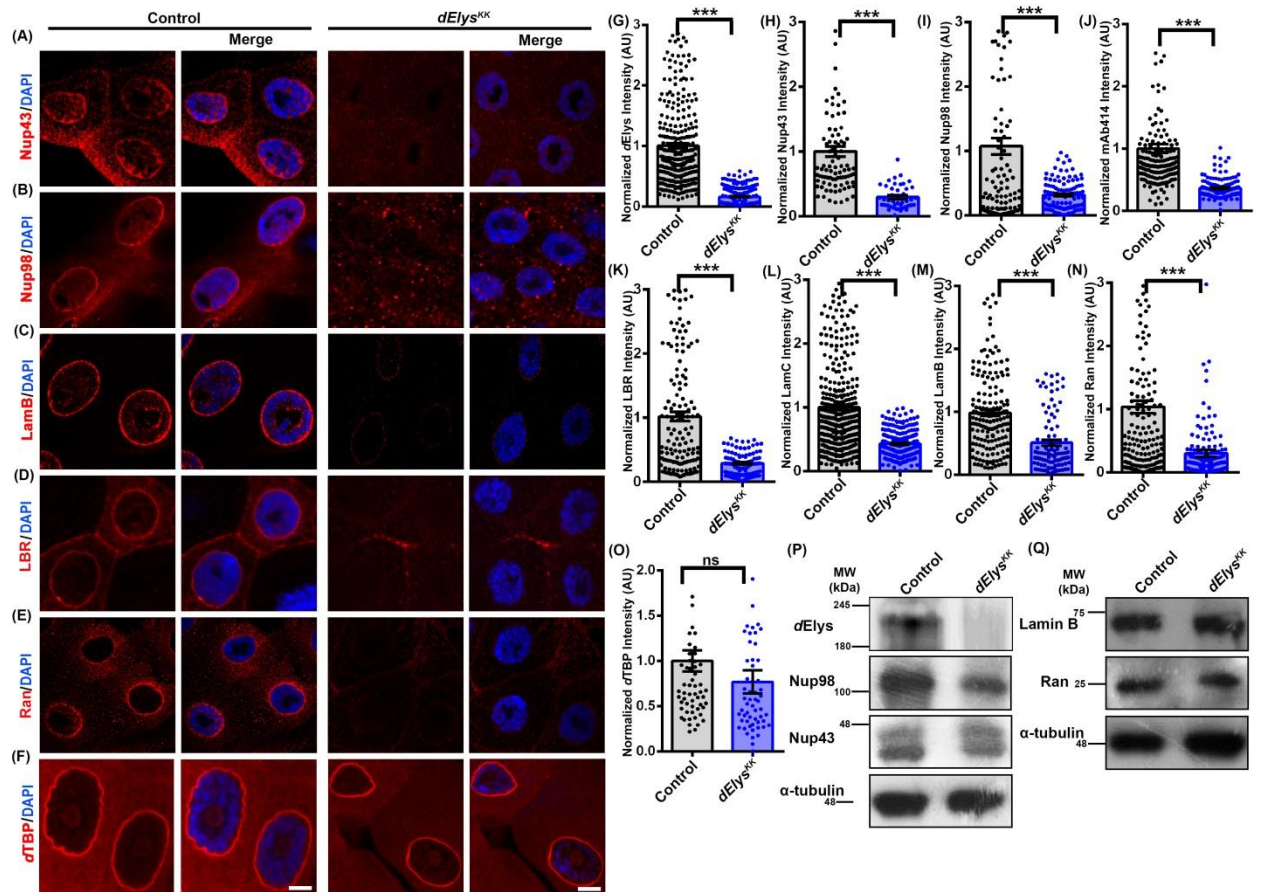


Figure S4: *dElys* depletion induces defects in nuclear pore complex and nuclear lamina but not the nuclear membrane

(A-E) Localization of Nup43, Nup98, Lamin B, LBR, and Ran on the nuclear rim assessed in control (first and second vertical columns) and *dElys* depleted (ubiquitous *Act5C*-GAL4 driven, third and fourth vertical columns) third instar larval salivary gland nuclei. DNA is stained with DAPI (Scale bar: 5 μm). Control is wild-type flies crossed with the *Act5C*-GAL4 driver.

(F) Staining of nuclear membrane-associated protein *dTBP* in third instar larval control and *dElys* depleted (ubiquitous *Act5C*-GAL4 driven) salivary gland nuclei (Scale bar: 5 μm).

(G-O) Quantitation of nuclear rim localization of *dElys*, Nup43, Nup98, mAb414, LBR, Lamin C, Lamin B, Ran, *dTBP* in control and *dElys* RNAi. The intensities of

each molecule were normalized against the intensity of DAPI. Data are represented from at least three independent experiments. At least 45 nuclei were analyzed from 7-8 pairs of salivary glands. Statistical significance derived from the student's t-test. Error bars represent SEM. ns is non-significant.

(P, Q) Western blot analysis to detect levels of indicated molecules in control and *dElys* knockdown (ubiquitous *Act5C-GAL4* driven) lysates prepared from third instar larva head complex. Nup98, Nup43, Lamin B and Ran were detected in stripes separated from blots used in Fig. 3. α -tubulin was used as a loading control. Control is wild-type flies crossed with the *Act5C-GAL4* driver. Each western is performed at least three times.

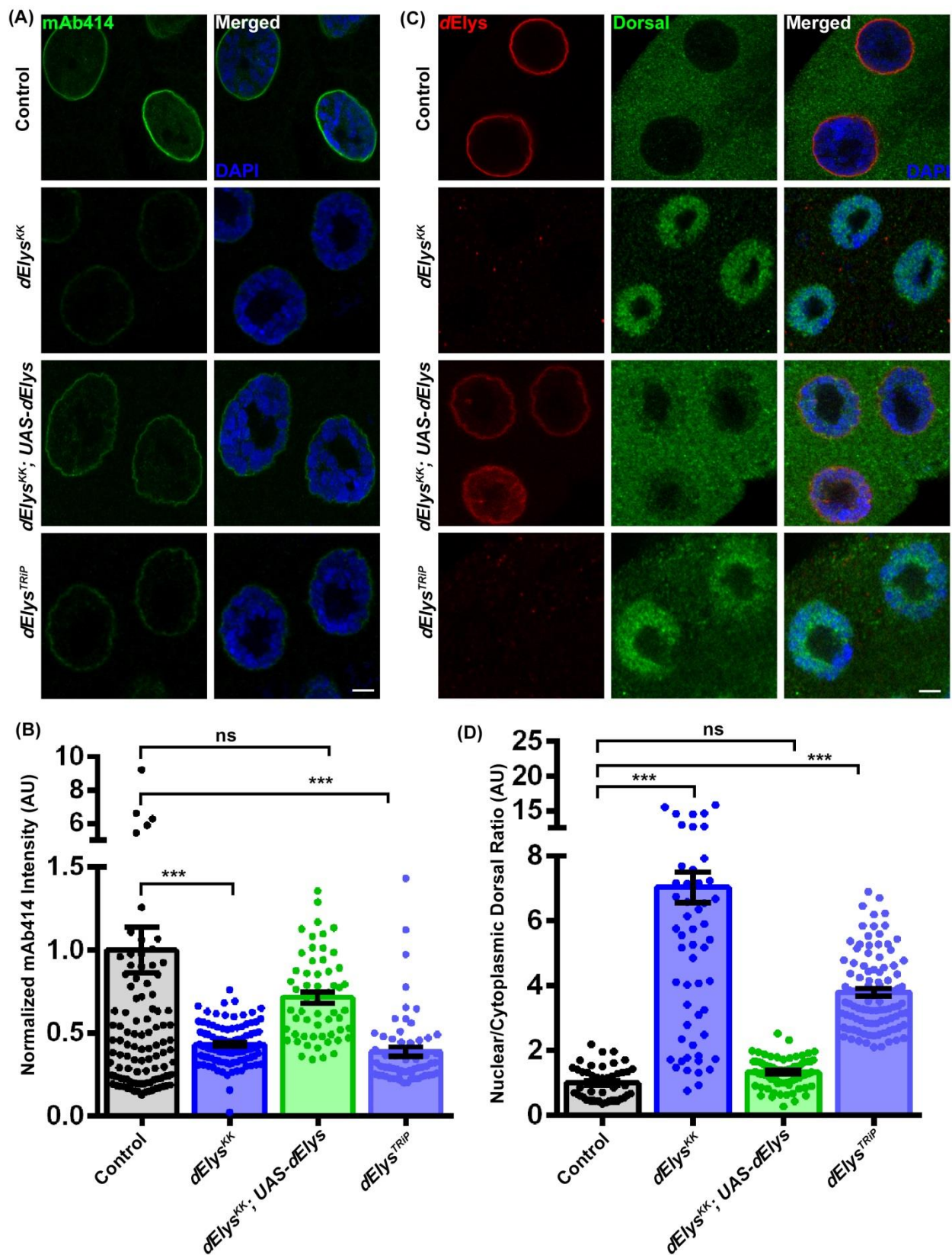


Figure S5: *dElys* depletion phenotype is consistent in both RNAi lines can be partially rescued by providing an extra copy of *dElys*

(A) Third instar larval salivary glands stained with mAb414 antibodies (FG-repeat nucleoporins, green) in control, *dElys*^{KK}, and *dElys*^{KK}; *UAS-dElys* and *dElys*^{TRiP} organisms. DNA is stained with DAPI. RNAi and *dElys* transgene were driven with ubiquitous *Act5C-GAL4* and salivary gland specific *fkh-GAL4*. Control is wild type flies crossed with *Act5C-GAL4*; *fkh-GAL4*. (Scale Bar: 5 μ m)

(B) The quantification of nuclear rim intensities of mAb414 from control, *dElys*^{KK}, and *dElys*^{KK}; *UAS-dElys* and *dElys*^{TRiP} salivary glands. Data are represented from at least three independent experiments. At least 45 nuclei were analyzed from 7-8 pairs of salivary glands. Statistical significance derived from one-way ANOVA followed by Tukey's post-hoc test. The error bar is SEM. *** represents $p < 0.0001$ and ns is non-significant.

(C) Detection of Dorsal (Green), and *dElys* (Red) localization in control, *dElys*^{KK}, and *dElys*^{KK}; *UAS-dElys* and *dElys*^{TRiP} organisms. DNA is stained with DAPI. RNAi and *dElys* transgene were driven with ubiquitous *Act5C-GAL4* and salivary gland specific *fkh-GAL4*. Control is wild type flies crossed with *Act5C-GAL4*; *fkh-GAL4*. (Scale Bar: 5 μ m)

(D) The quantification of nuclear Dorsal intensities from control, *dElys*^{KK}, and *dElys*^{KK}; *UAS-dElys* and *dElys*^{TRiP} salivary glands. Data are represented from at least three independent experiments. At least 45 nuclei were analyzed from 7-8 pairs of salivary glands. Statistical significance derived from one way ANOVA followed by Tukey's post-hoc test. The error bar is SEM. *** represents $p < 0.0001$ and ns is non-significant.

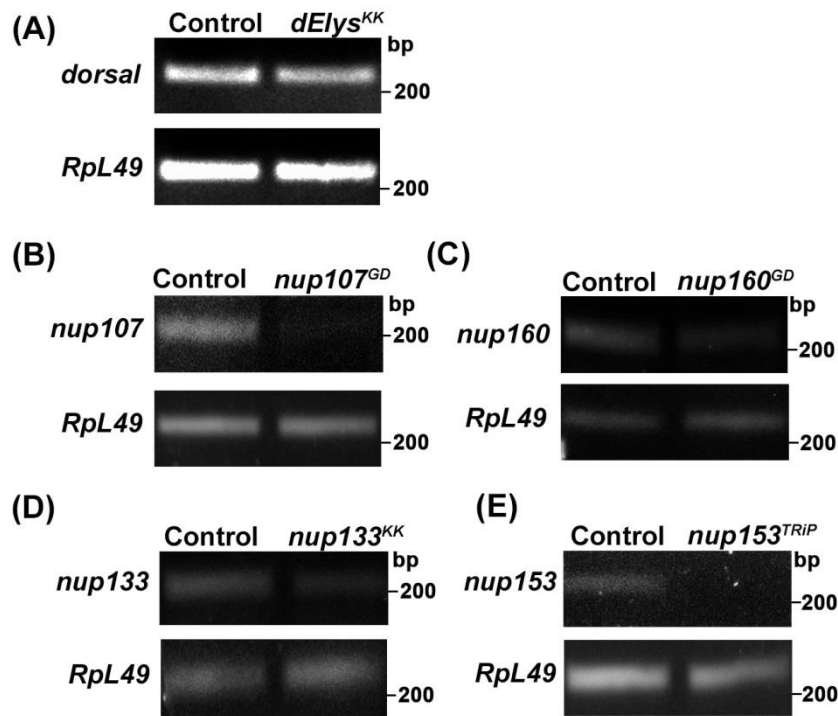


Figure S6: Expression analysis of other nucleoporins knockdown by RNAi lines

(A) Semiquantitative PCR analysis for expression of *dorsal* in control and *dElys* depleted cDNA. *RpL49* was used as an internal control gene. Data are derived from at least three independent experiments.

(B-E) Semi-quantitative PCR analysis of nucleoporins expression in their respective RNAi knockdown. *RpL49* was used as an internal control gene. Data are derived from at least three independent experiments.

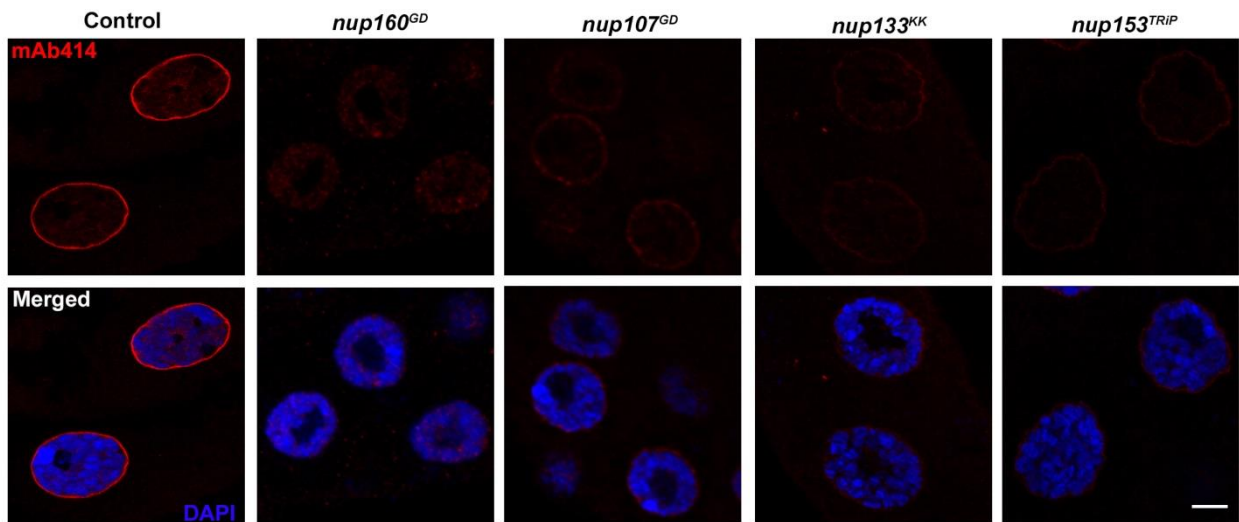


Figure S7: Depletion of other essential nucleoporins perturbs the NPC structure

mAb414 staining of third instar larval salivary gland nuclei from essential nucleoporin (mentioned above panels) depleted organisms. DNA is stained with DAPI (Scale bar: 5 μ m).

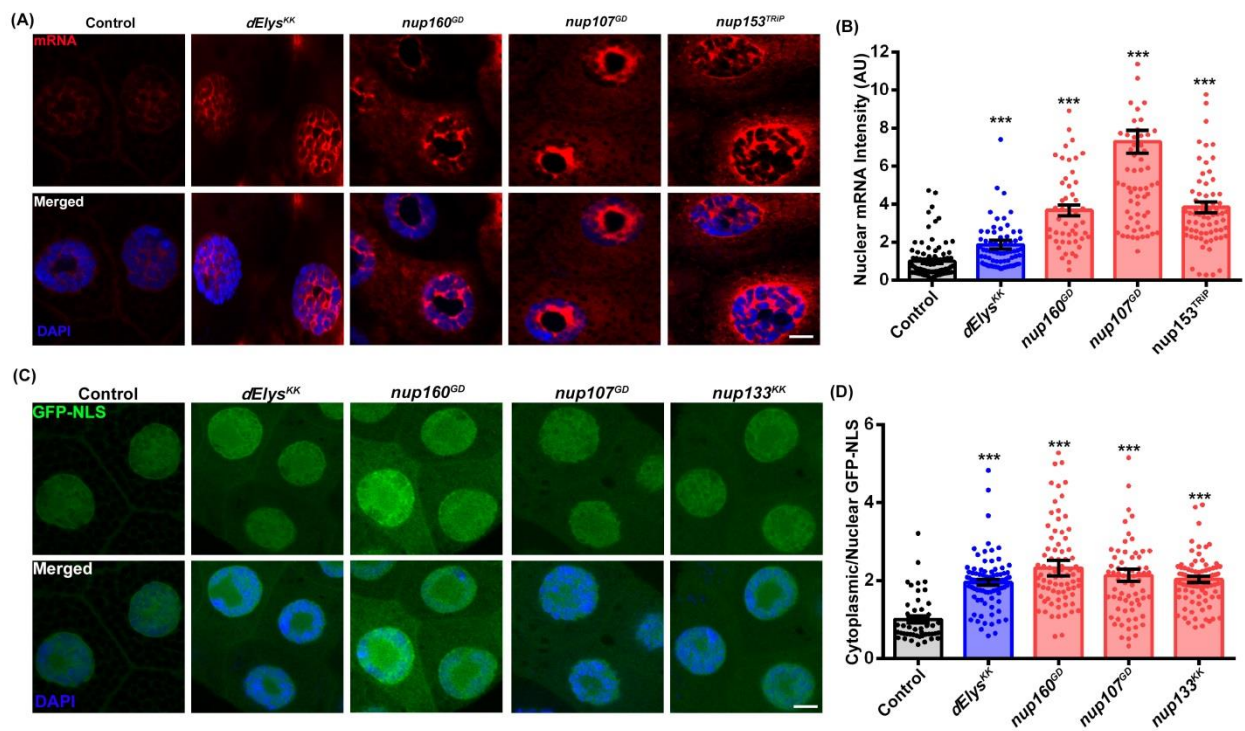


Figure S8: Depletion of other essential nucleoporins affects NPCs functions similar to *dElys* depletion

(A) mRNA-FISH based assessment of mRNA export in salivary gland nuclei of third instar larva from *dElys* and knockdown other indicated nucleoporins. DNA is stained with DAPI (Scale bar: 5 μ m).

(B) Quantification of the nuclear intensity of mRNA. Data are represented from at least three independent experiments. Statistical significance derived from one-way ANOVA followed by Tukey's post-hoc test. The error bar is SEM. *** represents $p < 0.0001$, ns is non-significant. At least 45 nuclei were analyzed from 7-8 pairs of salivary glands.

(C) Nuclear import defect assessment in third instar larval salivary glands by GFP-NLS localization in *dElys* and other indicated nucleoporin depletion. DNA is stained with DAPI (Scale bar: 5 μ m).

(D) Quantification of the cytoplasmic/nuclear intensity ratio of GFP-NLS showing a marked increase in GFP-NLS in the cytoplasm. Data are represented from at least three independent experiments. Statistical significance derived from one-way ANOVA followed by Tukey's post-hoc test. The error bar is SEM. *** represents $p < 0.0001$. At least 45 nuclei were analyzed from 7-8 pairs of salivary glands.

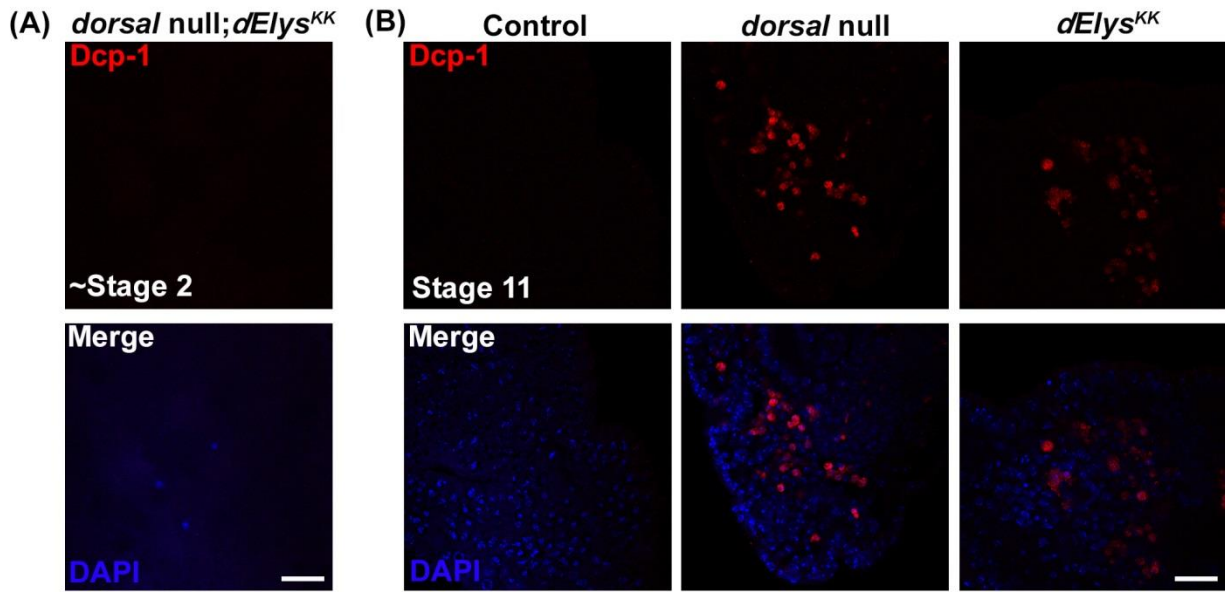


Figure S9: Loss of *dorsal* and *dElys* induces apoptosis in embryos

(A) Early embryonic growth defects in organisms from the combined loss of *dorsal* and *dElys* (*dorsal null; dElys^{KK}*) analyzed for induction of apoptosis using the Dcp-1 (red) antibody. DNA is stained with DAPI (Scale bar: 20 μ m).

(B) The anterior region of stage 11 embryos from in control, *dorsal* null, *dElys* depletion (*mat- α -tub-GAL4* driven) stained with Dcp-1 (red) for assessment of apoptotic response (Scale bar: 20 μ m).

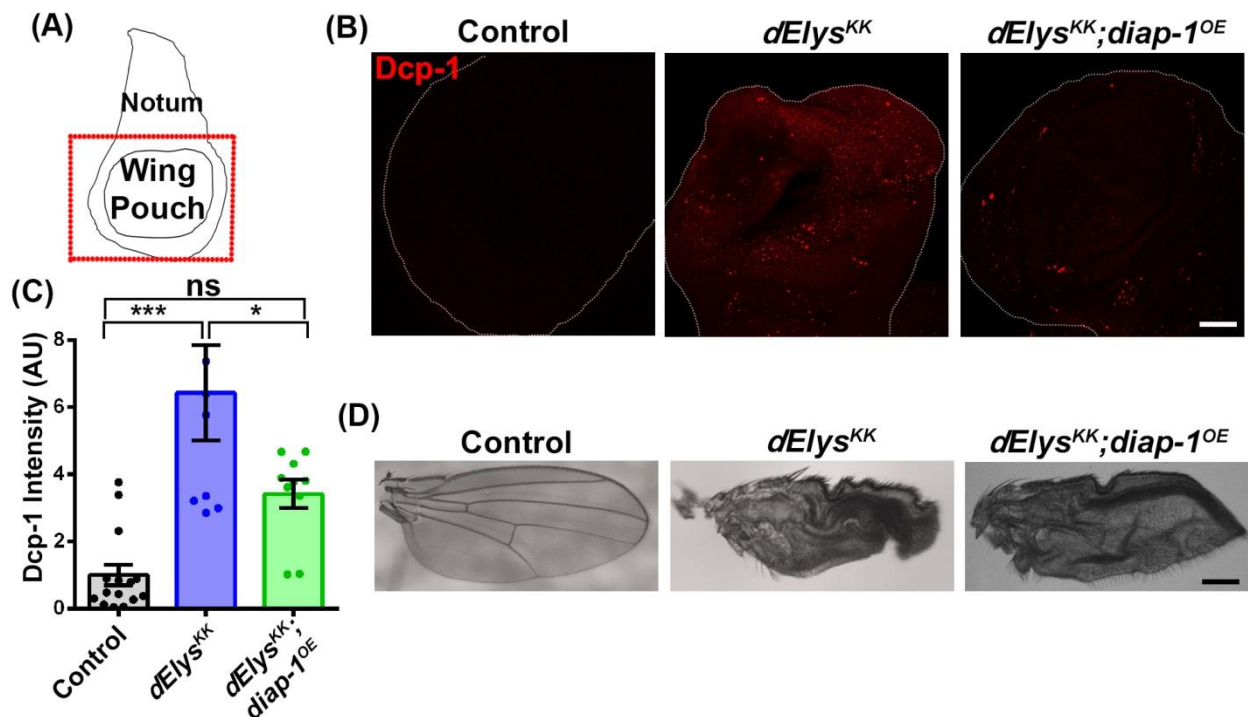


Figure S10: *diap-1* over-expression can partially rescue *dElys* depletion induced apoptotic phenotype in wings

(A) Schematic of wing imaginal disc from third instar larva highlighting the wing pouch area imaged in B

(B) Wing imaginal discs from control, *dElys* depletion, and *dElys^{KK}; diap-1^{OE}* third instar larva driven with *nubbin-GAL4*; *Ubx-GAL4* stained for Dcp-1. The shape of the wing imaginal disc is outlined for comparisons (Scale bar: 20 μ m).

(C) Quantitation of Dcp-1 intensity in wing pouch area in control, *dElys^{KK}* and *dElys^{KK}; diap-1^{OE}*. Data is derived from two independent experiments. Statistical significance derived from one way ANOVA followed by Tukey's post-hoc test. The error bar is SEM. *** represents $p < 0.0001$, * represents $p < 0.05$ and ns is non-significant.

(D) Adult wing from control, *dElys* depletion, and *dElys^{KK}; diap-1^{OE}* organisms as indicated. (Scale bar: 200 μ m).